European Journal of Nuclear Medicine and Molecular Imaging (2022) 49:1985–1996
https://doi.org/10.1007/s00259-021-05591-x

ORIGINAL ARTICLE

Fatty acid-conjugated radiopharmaceuticals for fibroblast activation protein-targeted radiotherapy

Pu Zhang[1] · Mengxin Xu[1] · Jie Ding[2] · Junyi Chen[1] · Taiping Zhang[3] · Li Huo[2] · Zhibo Liu[1,4]

Received: 12 July 2021 / Accepted: 11 October 2021 / Published online: 8 November 2021

Abstract

Introduction Radiopharmaceuticals that target cancer-associated fibroblasts (CAFs) have become an increasingly attractive strategy for cancer theranostics. Recently, a series of fibroblast activation protein inhibitor (FAPI)-based radiopharmaceuticals have been successfully applied to the diagnosis of a variety of cancers and exhibited excellent tumor selectivity. Nevertheless, CAF-targeted radionuclide therapy encounters difficulties in cancer treatment, as the tumor uptake and retention of FAPIs are insufficient. To meet this challenge, we tried to conjugate albumin-binding moiety to FAPI molecule for prolonged circulation that may increase the accumulation and retention of radiopharmaceuticals in tumor.

Methods Two fatty acids, lauric acid (C12) and palmitic acid (C16), were conjugated to FAPI-04 to give two albumin-binding FAPI radiopharmaceuticals, denoted as FAPI-C12 and FAPI-C16, respectively. They had been radiolabeled with gallium-68, yttrium-86, and lutecium-177 for stability study, binding affinity assay, PET and SPECT imaging, biodistribution, and radionuclide therapy study to systematically evaluate their potential for CAF-targeted radionuclide therapy.

Results FAPI-C12 and FAPI-C16 showed high binding affinity to FAP with the IC_{50} of 6.80 ± 0.58 nM and 5.06 ± 0.69 nM, respectively. They were stable in both saline and plasma. The tumor uptake of [^{68}Ga]Ga-FAPI-04 decreased by 56.9% until 30 h after treated with FAPI-C16 before, and the uptakes of [^{86}Y]Y-FAPI-C12 and [^{86}Y]Y-FAPI-C16 in HT-1080-FAP tumor were both much higher than that of HT-1080-Vehicle tumor which identified the high FAP specific of these two radiopharmaceuticals. Both FAPI-C12 and FAPI-C16 showed notably longer circulation and significantly enhanced tumor uptake than those of FAPI-04. [^{177}Lu]Lu-FAPI-C16 had the higher tumor uptake at both 24 h (11.22 ± 1.18%IA/g) and 72 h (6.50 ± 1.19%IA/g) than that of [^{177}Lu]Lu-FAPI-C12 (24 h, 7.54 ± 0.97%IA/g; 72 h, 2.62 ± 0.65%IA/g); both of them were much higher than [^{177}Lu]Lu-FAPI-04 with the value of 1.24 ± 0.54%IA/g at 24 h after injection. Significant tumor volume inhibition of [^{177}Lu]Lu-FAPI-C16 at the high activity of 29.6 MBq was observed, and the median survival was 28 days which was much longer than that of the [^{177}Lu]Lu-FAPI-04 treated group of which the median survival was only 10 days.

Conclusion This proof-of-concept study validates the hypothesis that conjugation of albumin binders may shift the pharmacokinetics and enhance the tumor uptake of FAPI-based radiopharmaceuticals. This could be a general strategy to transform the diagnostic FAP-targeted radiopharmaceuticals into their therapeutic pairs.

Keywords FAPI · Albumin binder · Radionuclide therapy

Pu Zhang, Mengxin Xu and Jie Ding contributed equally to this work.

This article is part of the Topical Collection on Theragnostic

✉ Li Huo
huoli@pumch.cn

✉ Zhibo Liu
zbliu@pku.edu.cn

[1] Radiochemistry and Radiation Chemistry Key Laboratory of Fundamental Science, Beijing National Laboratory for Molecular Sciences, College of Chemistry and Molecular Engineering, Peking University, 100871 Beijing, China

[2] Department of Nuclear Medicine, Peking Union Medical College Hospital, Chinese Academy of Medical Science & Peking Union Medical College, Beijing 100730, China

[3] Department of General Surgery, Peking Union Medical College Hospital, Chinese Academy of Medical Science & Peking Union Medical College, Beijing 100730, China

[4] Peking University-Tsinghua University Center for Life Sciences, Beijing 100871, China

Introduction

Tumor stroma which is composed of specialized connective tissue cells such as fibroblasts [1] and the extracellular matrix (ECM) [2] is essential in cancer development, progression, and metastasis [3]. As one major cellular component in tumor stroma, cancer-associated fibroblasts (CAFs) cells which are an established source of classical tumor-promoting growth factors [4, 5] make the tumor cells exhibit more aggressive and result the poor prognosis [6]. Considering the important role in cancer development, CAF-targeted diagnosis and therapy have become an important strategy for cancer management [7, 8]. Fibroblast activation protein (FAP), a dual specificity serine protease [9], which is overly expressed in CAFs but notably less expressed in normal tissues, allows the selective targeting of CAFs in many cancers [10], and has become a pivotal biomarker for CAF-targeted treatment [11, 12].

Since 2018, a series of fibroblast activation protein inhibitor (FAPI)-based radiopharmaceuticals including [^{68}Ga]Ga-FAPI-02 [13] and [^{68}Ga]Ga-FAPI-04 [14] have been developed and performed excellent FAP-targeted diagnosis outcomes in the clinical studies [15–17]. To make these FAPI based radiopharmaceuticals more suitable for radionuclide therapy, Loktev and co-workers focused on the direct chemical structure optimization and developed FAPI-21 and FAPI-46 to further increase the tumor uptake and retention for therapeutic outcome improving [18, 19]. Though only the [^{177}Lu]Lu-FAPI-21 has an enhanced tumor retention when comparing with [^{177}Lu]Lu-FAPI-04, with the tumor uptake of 6.03 ± 0.68%IA/g and 2.86 ± 0.31%IA/g respectively at 24 h after injection [18], the rapid clearance from the circulation and the insufficient tumor accumulation still hamper the further application of FAPI radiopharmaceuticals for cancer therapy. A promising strategy to meet the challenge may be to prolong the blood circulation by conjugating FAPI with the albumin-binding moieties as illustrated by a series of studies that the radiopharmaceuticals conjugated with Evans blue [20, 21] or 4-(p-iodophenyl) butyric acid [22, 23] moieties can significantly improve the therapeutic dose delivery [24].

Besides these popular albumin-binding moieties, fatty acids are also a type of classic albumin-binding moieties. Liraglutide [25], the fatty acid conjugate, has been approved by FDA and used in clinics to elongate the blood circulation of the insulin and glucagon-like peptide-1 analogs [26, 27]. For the reason that the structure activity and protraction relationship of the fatty acid alky chain length, polarity, and bulkiness have been thoroughly investigated which provides us more regular information for rational selection and optimal design [28, 29], we are wondering whether fatty acid-conjugated FAPI would have sufficient tumor uptake and retention to match the half-lives of therapeutic radionuclides (e.g., lutecium-177).

There are studies suggesting that conjugations with palmitic acid (C16) often have longer blood circulation than other fatty acids [28]. Yet conjugation with lauric acid (C12) had also been investigated in this work, as it may have a better balance between blood clearance and tumor accumulation. In this study, we designed and synthesized FAPI-C12 (Fig. 1A) and FAPI-C16 (Fig. 1B), two fatty acid-FAPI conjugates, to extend its blood retention time and maximize the uptake in FAP-expressing tumors. Head-to-head comparisons between radiolabeled FAPI-C12 and FAPI-C16 were conducted by in vitro competition binding, as well as by PET and SPECT imaging, biodistribution, and endoradiotherapy studies in FAP-expressing xenografts bearing mice. With greatly enhanced tumor uptake and treatment efficacy compared to [^{177}Lu]Lu-FAPI-04 in preclinical studies, [^{177}Lu]Lu-FAPI-C16 warrants further investigation for FAP-targeted radionuclide therapy.

Materials and methods

Ligands and radionuclides

FAPI-C12 and FAPI-C16 were synthesized according to the methods illustrated in the supporting information. Gallium-68 was obtained as $^{68}GaCl_3$ by eluting the ^{68}Ge-^{68}Ga generator (iThemba LABS, South Africa) using 0.6 M HCl solution. Yttrium-86 was obtained as $^{86}YCl_3$ in 0.1 M HCl solution, the target design followed our previous report [30], and the purification procedure followed the method reported previously by using one 14 MeV cyclotron [31]. $^{177}LuCl_3$ (ITG, Germany) in 0.1 M HCl solution was purchased from China Isotope & Radiation Corporation.

Radiolabeling and stability in vitro

For all the radiolabeling processes, 50 nmol FAPI-C12 or FAPI-C16 was used. For ^{68}Ga labeling, 256–354 MBq $^{68}GaCl_3$ in 0.6 M HCl (1 mL) was adjusted to pH 4.5 by using the solution of Na_2CO_3 (3 M) and NaOH (3 M); the mixture was incubated at 90 ℃ for 10 min. For ^{86}Y labeling, 105–142 MBq $^{86}YCl_3$ in 0.1 M HCl (1 mL) was adjusted to pH 4.5 by using the solution of Na_2CO_3 (3 M); the mixture was incubated at 90 ℃ for 10 min. For ^{177}Lu labeling, 158–231 MBq $^{177}LuCl_3$ in 0.1 M HCl was added into the FAPI-C12 or FAPI-C16 in NaOAc buffer (0.2 M, pH 4.5–5.0) and then incubated at 90 ℃ for 15 min. pH-indicator strips were used to detect the pH of the labeling mixture. Sep-Pak Light C18 cartridges (Waters) activated by ethanol and water were used for purification,

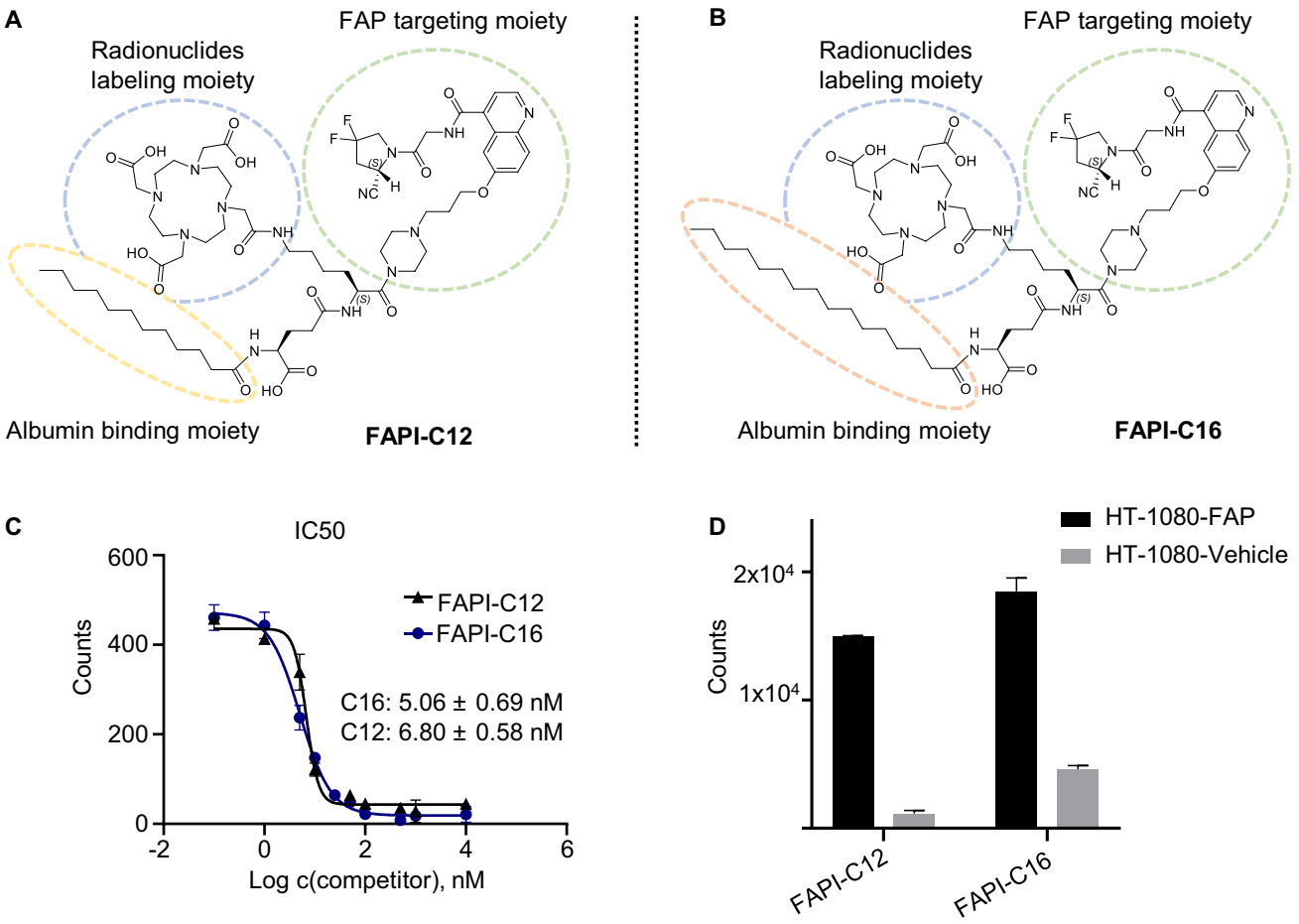

Fig. 1 **A, B** Chemical structure of FAPI-C12 and FAPI-C16; **C** cell competition assays of FAPI-C12 and FAPI-C16 using HT-1080-FAP cells; **D** cell uptake assays of [^{68}Ga]Ga-FAPI-C12 and [^{68}Ga]Ga-FAPI-C16

and the quality control was performed by using a radioactivity detector equipped with high-performance liquid chromatography (radio-HPLC). For stability study, the radiochemical purity of [^{177}Lu]Lu-FAPI-C12 and [^{177}Lu]Lu-FAPI-C16 incubated in saline and human serum were measured using radio-HPLC at 24 h, 72 h, and 120 h, respectively. For stability study in serum, an equivalent volume of acetonitrile was added to the mixture twice to precipitate the serum thoroughly and then centrifuged; the supernatant was analyzed by radio-HPLC. The radio-HPLC method was as follows: 10% acetonitrile containing 0.1% TFA during 0–2 min; 10–60% acetonitrile containing 0.1% TFA during 2–10 min; 60% acetonitrile containing 0.1% TFA during 10–12 min; and 60–10% acetonitrile containing 0.1% TFA during 12–15 min. The flow rate was 1 mL/min, and the C18 column (4.6 × 150 mm, 5 μm, XBridge, Waters) was used for chromatograms collection.

Cell culture and assay

The cell lines HT-1080-Vehicle (mock-transfected human fibrosarcoma cell line) and HT-1080-FAP which is the human fibrosarcoma cell line transferred with the human FAP gene were used for cell assays and other experiments in vitro and in vivo. Eagle's minimum essential medium (EMEM, Hyclone) containing 10% fetal bovine serum (FBS, Corning), 1% antibiotic–antimycotic (Anti-Anti, Invitrogen), and 4 μg/mL Blasticidin S (Pharmabiology) was used for cell cultivation. For competition assays, HT-1080-FAP cells seeded in 6-well plates were incubated with [^{68}Ga]Ga-FAPI-04 and unlabeled FAPI-C12 or FAPI-C16 (10^{-5}-10^{-9} M) simultaneously in the fresh medium without FBS for 1 h in the cell incubator. When the incubation finished, the medium was removed, and the cells were washed with PBS (1 mL) twice; then the cells were lysed with NaOH

(1 M, 0.5 mL) and washed with PBS (0.5 mL) twice, collected the NaOH (0.5 mL) and PBS (0.5 mL × 2) solution together, and detected the radioactive counts as the uptake of [^{68}Ga]Ga-FAPI-04. For uptake assays, HT-1080-Vehicle and HT-1080-FAP cells seeded in 6-well plates were incubated with [^{68}Ga]Ga-FAPI-C12 or [^{68}Ga]Ga-FAPI-C16 in the fresh medium without FBS for 1 h in cell incubator; when the incubation finished, the cells were processed following the protocol used in the competition assays.

Tumor xenograft model

All animal care and experimental procedure were performed following the guidelines of the care and use of laboratory animals approved by the ethics committee of Peking University. Six-weeks-old female nu/nu mice purchased from Beijing Vital River Laboratory Animal Technology Co., Ltd. For HT-1080-FAP tumor-bearing mice preparation, the mice were subcutaneously inoculated about 5×10^6 HT-1080-FAP cells into the shoulder. For HT-1080-Vehicle tumor-bearing mice preparation, the mice were subcutaneously inoculated about 5×10^6 HT-1080-Vehicle cells into the shoulder.

Small animal PET and SPECT imaging

Small animal PET/CT and SPECT/CT (Mediso imaging system) were used for PET and SPECT scan, image instruction, and data analysis. The whole-body dynamic PET images of [^{68}Ga]Ga-FAPI-C12 and [^{68}Ga]Ga-FAPI-C16 were collected using HT-1080-FAP tumor-bearing mice. Scan of the first hour was acquired after intravenous injection of about 22.2 MBq [^{68}Ga]Ga-FAPI-C12 or [^{68}Ga]Ga-FAPI-C16; then a 15-min scan was performed every hour until 4 h after injection. Whole-body PET imaging of [^{86}Y]Y-FAPI-C12 and [^{86}Y]Y-FAPI-C16 was performed using HT-1080-FAP tumor-bearing mice at 1 h, 6 h, 12 h, 24 h, 36 h, and 48 h after intravenous injection of about 7.4 MBq [^{86}Y]Y-FAPI-C12 or [^{86}Y]Y-FAPI-C16. The whole-body PET images of HT-1080-Vehicle tumor-bearing mice were collected at 12 h, 24 h, and 48 h after intravenous injection of about 7.4 MBq [^{86}Y]Y-FAPI-C12 or [^{86}Y]Y-FAPI-C16. For the blocking study, HT-1080-FAP tumor-bearing mice were performed [^{68}Ga]Ga-FAPI-04 PET imaging firstly; then the mice were treated with about 500 μg unlabeled FAPI-C16; after 6 h and 30 h, the same mice were performed [^{68}Ga]Ga-FAPI-04 PET imaging again. SPECT imaging of [^{177}Lu]Lu-FAPI-C12 and [^{177}Lu]Lu-FAPI-C16 was performed using HT-1080-FAP tumor-bearing mice at 4 h, 24 h, and 48 h after intravenous injection of about 37.0 MBq [^{177}Lu]Lu-FAPI-C12 or [^{177}Lu]Lu-FAPI-C16. SPECT imaging of [^{177}Lu]Lu-FAPI-04 was also performed at 24 h after injection.

Biodistribution study

A biodistribution study was performed using HT-1080-FAP tumor-bearing mice. At 24 h and 72 h after intravenous injection of about 1110 kBq [^{177}Lu]Lu-FAPI-C12 and [^{177}Lu]Lu-FAPI-C16, the mice were sacrificed and anatomized; the radioactive counts and the weight of main organs and tissues were measured. The data were normalized to %IA/g using the 1% of total injection counts. Biodistribution study of [^{177}Lu]Lu-FAPI-04 was also performed using HT-1080-FAP tumor-bearing mice at 24 h after injection.

Radionuclide therapy study

A radionuclide therapy study was performed using HT-1080-FAP tumor-bearing mice. When the average tumor volume reached about 100 mm^3, the mice were divided into five groups, and there were six mice in every group. Groups A, B, C, D, and E were treated respectively with 29.6 MBq [^{177}Lu]Lu-FAPI-C16, 18.5 MBq [^{177}Lu]Lu-FAPI-C16, 29.6 MBq [^{177}Lu]Lu-FAPI-C12, 29.6 MBq [^{177}Lu]Lu-FAPI-04, and saline. The mice were euthanized when the tumor volume reached above 1000 mm^3, or the body weight decreased by 10%, or ulcerated.

Histopathologic staining

The main organs including the heart, liver, spleen, lung, kidney, and intestine of the mice treated with saline, [^{177}Lu]Lu-FAPI-04, [^{177}Lu]Lu-FAPI-C12, and [^{177}Lu]Lu-FAPI-C16 were performed hematoxylin and eosin (H&E) staining following the previous study [32]. The tumors of the mice were performed immunohistochemistry (IHC) staining, and Anti-human FAP mAb (Abcam) was used as the primary antibody.

Results

Radiochemistry and stability in vitro

For radiolabeling with ^{68}Ga, ^{86}Y, and ^{177}Lu, the radiochemical yields were over 90%, and the radiochemical purity of these radiolabeling products used for all the in vivo and in vitro studies was over 98% according to radio-HPLC. For [^{68}Ga]Ga-FAPI-C12 and [^{68}Ga]Ga-FAPI-C16, the specific activity was 4.4–5.9 GBq/μmol. For [^{86}Y]Y-FAPI-C12 and [^{86}Y]Y-FAPI-C16, the specific activity was 1.9–2.6 GBq/μmol. For [^{177}Lu]Lu-FAPI-C12 and [^{177}Lu]Lu-FAPI-C16, the specific activity was 3.0–4.4 GBq/μmol. As illustrated in Supplemental Figure 1, no free lutecium-177 was detected, and only the initial peaks of [^{177}Lu]Lu-FAPI-C12 and [^{177}Lu]Lu-FAPI-C16 were observed until 120 h after

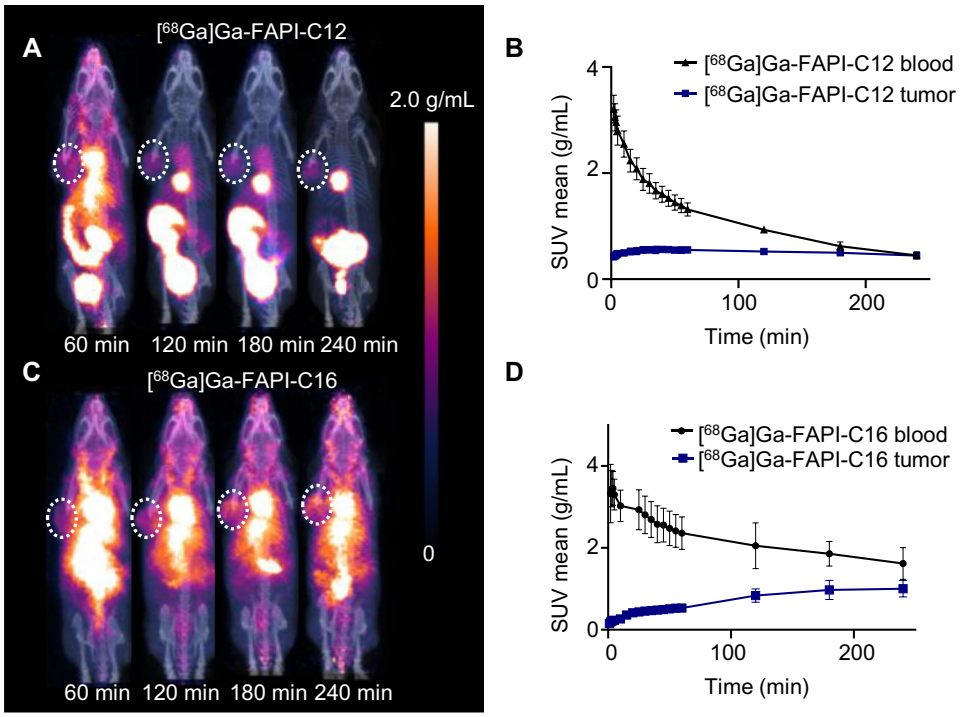

Fig. 2 **A, C** Dynamic PET imaging of [68Ga]Ga-FAPI-C12 and [68Ga]Ga-FAPI-C16; **B, D** corresponding blood and tumor time activity curves

incubation in saline and human serum and demonstrated that [177Lu]Lu-FAPI-C12 and [177Lu]Lu-FAPI-C16 both had excellent stability in saline and human serum.

Binding affinity assay

To evaluate the FAP specificity of these two radiopharmaceuticals, competition assays were performed by using the unlabeled FAPI-C12 and FAPI-C16 to compete with the uptake of [68Ga]Ga-FAPI-04. As illustrated in Fig. 1C, the uptake of [68Ga]Ga-FAPI-04 decreased significantly when using FAPI-C12 and FAPI-C16 at low concentrations which demonstrated that both FAPI-C12 and FAPI-C16 had high FAP specificity in vitro. The ligand concentration required for 50% inhibition (IC_{50}) of [68Ga]Ga-FAPI-04 uptake was 6.80 ± 0.58 nM and 5.06 ± 0.69 nM for FAPI-C12 and FAPI-C16, respectively. To further evaluate the FAP specificity in vitro, uptake assays were performed by using HT-1080-Vehicle cells as a control group; as illustrated in Fig. 1D, the uptakes of [68Ga]Ga-FAPI-C12 and [68Ga]Ga-FAPI-C16 in HT-1080-FAP cells were both significantly higher than that in HT-1080-Vehicle cells, which also verified the excellent FAP specificity of these two radiopharmaceuticals in vitro.

Pharmacokinetics study

Whole-body dynamic PET images of [68Ga]Ga-FAPI-C12 and [68Ga]Ga-FAPI-C16 using HT-1080-FAP tumor-bearing mice were collected firstly to preliminarily evaluate and compare their pharmacokinetics in healthy mice. As illustrated in Fig. 2, for [68Ga]Ga-FAPI-C12, the gallbladder and intestine uptake were extremely high which indicated that this radiopharmaceutical was metabolized and excreted rapidly through the liver, gallbladder, and intestine, while for [68Ga]Ga-FAPI-C16, the radioactivity signal was mainly concentrated in the heart and main blood vessels until 4 h after injection, indicating that [68Ga]Ga-FAPI-C16 had a longer plasma half-life in vivo than that of [68Ga]Ga-FAPI-C12. Metabolism of [68Ga]Ga-FAPI-C16 in the intestine was also clearly observed, but there was no obvious gallbladder uptake during all the time points. ROI (region of interest) analysis showed that the tumor uptake of [68Ga]Ga-FAPI-C16 (SUV mean: 0.53 ± 0.07) caught up with [68Ga]Ga-FAPI-C12 (SUV mean: 0.55 ± 0.05) at just 1 h after injection; then it increased continuously, while for [68Ga]Ga-FAPI-C12, the tumor uptake decreased gradually, resulting that the tumor uptake of [68Ga]Ga-FAPI-C16 was higher than that of [68Ga]Ga-FAPI-C12 during the subsequent time periods.

PET imaging

Whole-body PET images of [86Y]Y-FAPI-C12 and [86Y]Y-FAPI-C16 using HT-1080-FAP tumor-bearing mice were also collected for the purpose to monitor the pharmacokinetic behavior of these two radiopharmaceuticals during a longer time scale as the yttrium-86 has the appropriate half-life of 14.7 h. As illustrated in Fig. 3, imaging results of 1 h after injection were consistent with the dynamic

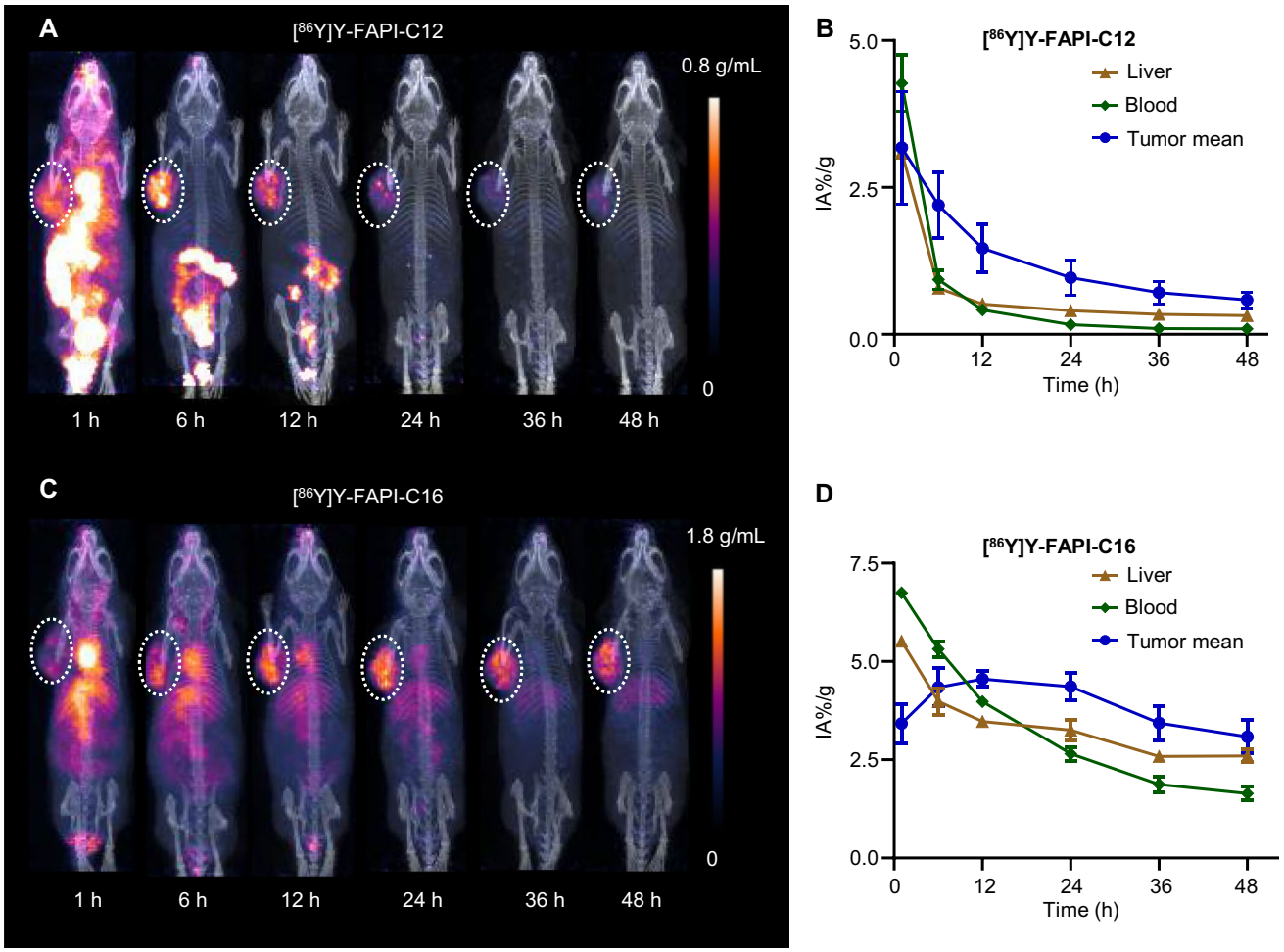

Fig. 3 **A, C** PET imaging of [^{86}Y]Y-FAPI-C12 and [^{86}Y]Y-FAPI-C16; **B, D** corresponding liver, blood, and tumor time activity curves

PET imaging. For [^{86}Y]Y-FAPI-C12, maximum tumor uptake was observed at 1 h after injection with the SUV value of 0.64 ± 0.19 and then decreased gradually, reaching the value of 0.44 ± 0.11 at 6 h and 0.12 ± 0.03 at 48 h after injection. The blood and liver uptake of [^{86}Y]Y-FAPI-C12 both decreased rapidly from 1 to 6 h with the value of 0.85 ± 0.10 to 0.19 ± 0.03 for blood uptake and 0.62 ± 0.02 to 0.16 ± 0.02 for liver uptake, resulting that the tumor to blood and tumor to liver ratios at 6 h after injection were 2.32 and 2.75, respectively. For [^{86}Y]Y-FAPI-C16, the tumor uptake increased gradually from 1 to 12 h with the SUV value of 0.68 ± 0.10 to 0.91 ± 0.04 and then decreased slowly, reaching the value of 0.87 ± 0.07 at 24 h and 0.62 ± 0.08 at 48 h after injection. The blood and liver uptake of [^{86}Y]Y-FAPI-C16 also decreased gradually from 1 to 24 h with the value of 1.35 ± 0.01 to 0.53 ± 0.03 for blood uptake and 1.10 ± 0.02 to 0.65 ± 0.05 for liver uptake, resulting that the tumor to blood and tumor to liver ratios were 1.64 and 1.34, respectively. For [^{86}Y]Y-FAPI-C12, clearly visible metabolism in the intestine continued up to 12 h after injection, while for [^{86}Y]Y-FAPI-C16, radioactivity signal was mainly enriched in the tumor, heart, and blood vessels, resulting in the much slower clearing out than [^{86}Y]Y-FAPI-C12.

Blocking experiment

To identify the in vivo FAP specificity of these two radiopharmaceuticals, whole-body PET imagings of [^{86}Y]Y-FAPI-C12 and [^{86}Y]Y-FAPI-C16 using HT-1080-Vehicle and HT-1080-FAP tumor-bearing mice were performed at 12 h, 24 h, and 48 h after injection. As illustrated in Fig. 4, the tumor uptakes of [^{86}Y]Y-FAPI-C12 and [^{86}Y]Y-FAPI-C16 in HT-1080-FAP tumor-bearing mice were much higher than that of HT-1080-Vehicle tumor-bearing mice until 24 h after injection, which demonstrated the high FAP specificity of these two radiopharmaceuticals in vivo. To further investigate the FAP specificity and tumor retention ability of FAPI-C16, a blocking study was also performed. As illustrated in Fig. 5, for the mice that had been treated with unlabeled FAPI-C16 before

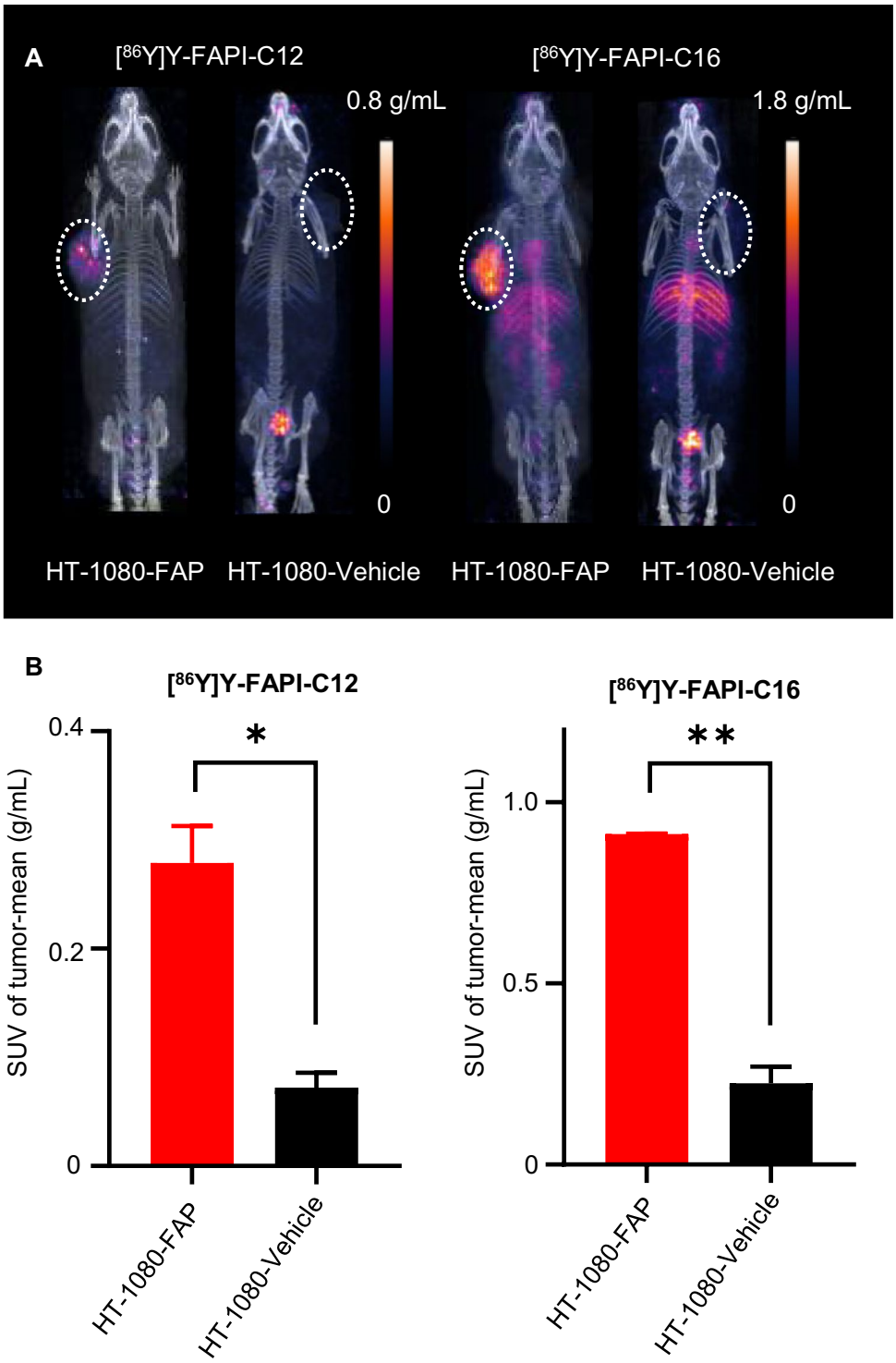

Fig. 4 **A** PET imaging of HT-1080-FAP and HT-1080-Vehicle tumor-bearing mice using [^{86}Y]Y-FAPI-C12 and [^{86}Y]Y-FAPI-C16; **B** tumor uptake comparison of HT-1080-FAP and HT-1080-Vehicle tumors

(SUV mean: 0.58), the tumor uptake of [^{68}Ga]Ga-FAPI-04 decreased by 56.9% until 30 h (SUV mean: 0.25) after treatment, which validated that FAPI-C16 remained the excellent FAP specificity during the circulation period, and the prolonged tumor retention mainly depended on the excellent FAP specificity and targeting ability of FAPI-C16 in vivo.

SPECT imaging

Whole-body SPECT imagings of [^{177}Lu]Lu-FAPI-C12, [^{177}Lu]Lu-FAPI-C16, and [^{177}Lu]Lu-FAPI-04 were also performed for the purpose to monitor and compare the in vivo pharmacokinetic behavior of these radiopharmaceuticals used for therapy. As illustrated in Fig. 6 and Supplemental

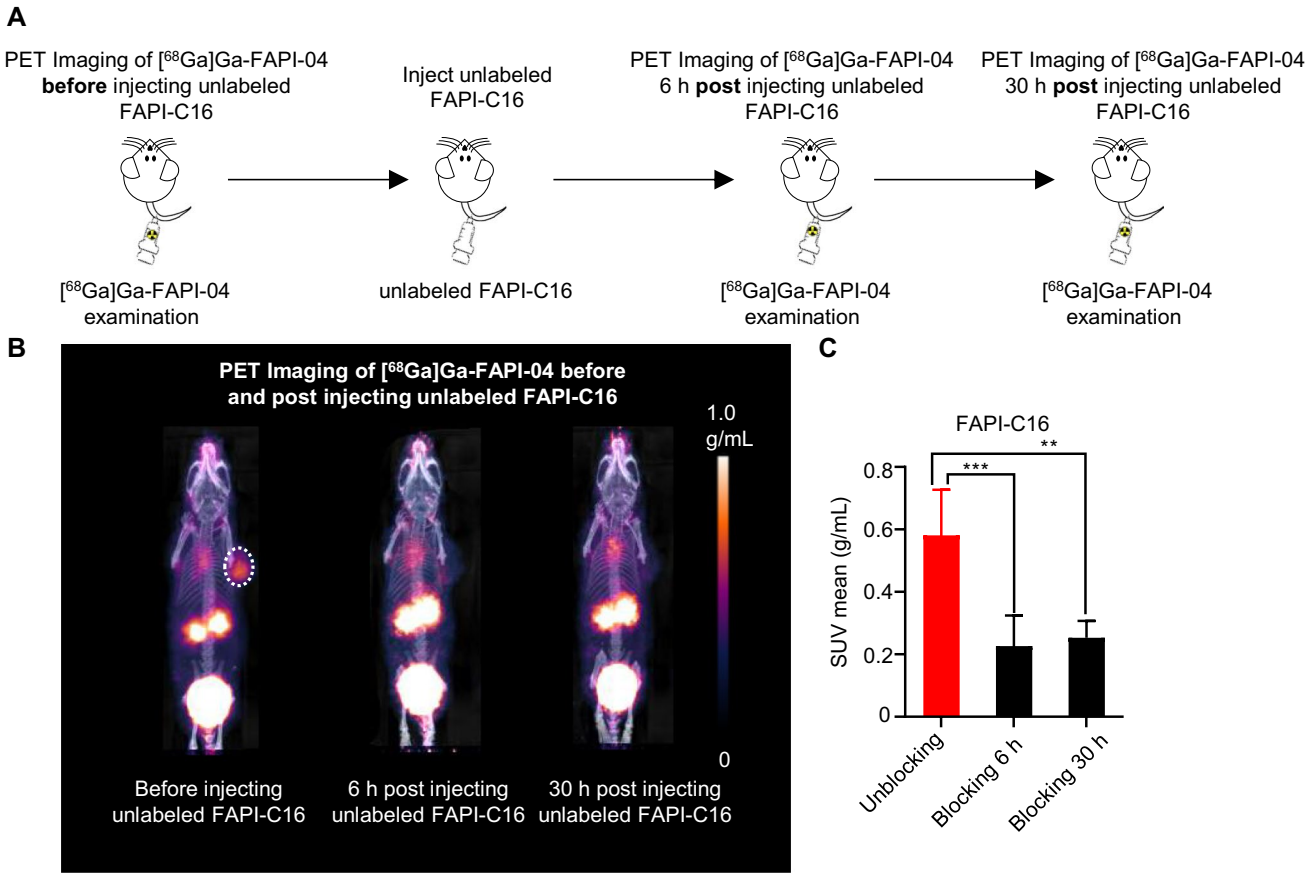

Fig. 5 **A** Protocol design of blocking study; **B** [^{68}Ga]Ga-FAPI-04 PET imaging before and at 6 h, 30 h after treated with unlabeled FAPI-C16; **C** corresponding ROI analysis of tumor uptake. $^{***}P < 0.001$

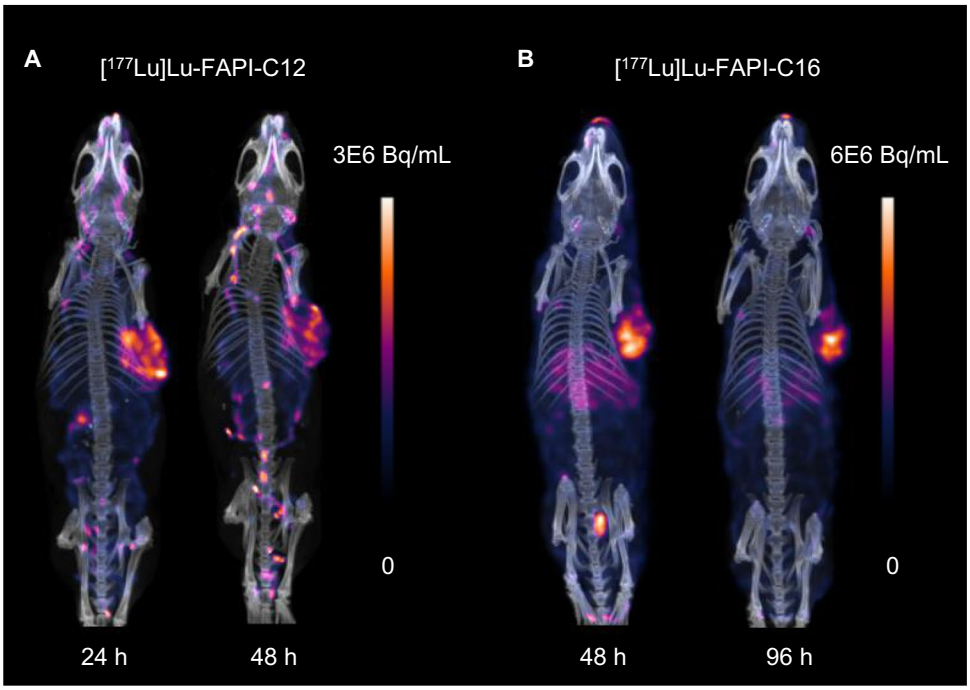

Fig. 6 SPECT imaging of [^{177}Lu]Lu-FAPI-C12 (**A**) and [^{177}Lu]Lu-FAPI-C16 (**B**) using HT-1080-FAP tumor-bearing mice

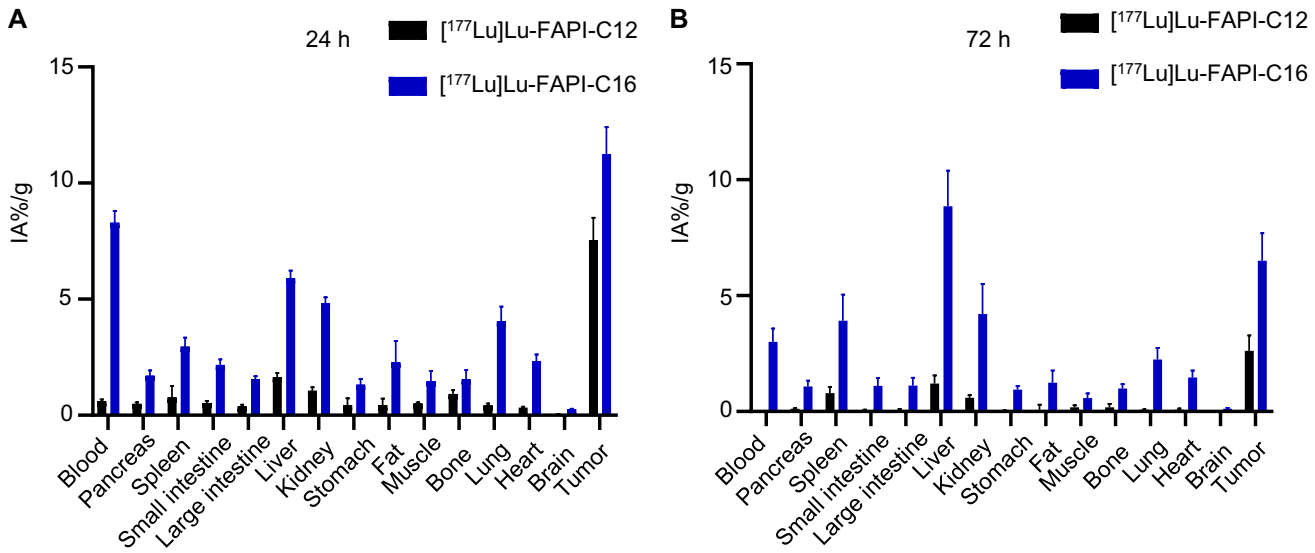

Fig. 7 Biodistribution study of [^{177}Lu]Lu-FAPI-C12 and [^{177}Lu]Lu-FAPI-C16 in HT-1080-FAP tumor-bearing mice at 24 h (**A**) and 72 h (**B**) after injection, $n = 5$

Figure 2, the tumor retention of [^{177}Lu]Lu-FAPI-C16 was much better than that of [^{177}Lu]Lu-FAPI-C12; meanwhile, the liver uptake of [^{177}Lu]Lu-FAPI-C16 was also higher, results of which were consistent with yttrium-86 PET imaging, while for [^{177}Lu]Lu-FAPI-04, there was almost no radioactivity signal that could be detected at 24 h after injection which indicated the much faster clearance of this radiopharmaceutical.

Biodistribution study

To further quantitatively evaluate and compare the in vivo pharmacokinetic properties of these two radiopharmaceuticals, biodistribution study of [^{177}Lu]Lu-FAPI-04, [^{177}Lu]Lu-FAPI-C12, and [^{177}Lu]Lu-FAPI-C16 was performed using HT-1080-FAP tumor-bearing mice. As illustrated in Fig. 7 and Table 1, [^{177}Lu]Lu-FAPI-C12 and [^{177}Lu]Lu-FAPI-C16 both had much higher tumor

Table 1 Biodistribution study results of [^{177}Lu]Lu-FAPI-C12 and [^{177}Lu]Lu-FAPI-C16 in HT-1080-FAP tumor-bearing mice at 24 h (**A**) and 72 h (**B**) after injection, $n = 5$

Organs	[^{177}Lu]Lu-FAPI-C12				[^{177}Lu]Lu-FAPI-C16			
	24 h		72 h		24 h		72 h	
	Mean(%IA/g)	SD(%IA/g)	Mean(%IA/g)	SD(%IA/g)	Mean(%IA/g)	SD(%IA/g)	Mean(%IA/g)	SD(%IA/g)
Blood	0.61	0.07	0.01	0.00	8.29	0.50	3.01	0.58
Pancreas	0.49	0.06	0.12	0.03	1.70	0.22	1.08	0.25
Spleen	0.77	0.49	0.79	0.26	2.95	0.39	3.92	1.12
Small intestine	0.53	0.08	0.04	0.04	2.17	0.23	1.10	0.33
Large intestine	0.38	0.07	0.02	0.09	1.56	0.12	1.12	0.33
Liver	1.64	0.17	1.20	0.35	5.90	0.33	8.85	1.53
Kidney	1.06	0.15	0.59	0.11	4.83	0.25	4.21	1.29
Stomach	0.44	0.29	0.04	0.02	1.32	0.23	0.94	0.15
Fat	0.43	0.28	-0.16	0.46	2.28	0.91	1.24	0.53
Muscle	0.51	0.06	0.18	0.09	1.46	0.44	0.58	0.20
Bone	0.91	0.17	0.18	0.15	1.55	0.40	0.99	0.19
Lung	0.44	0.07	0.08	0.02	4.04	0.64	2.24	0.50
Heart	0.33	0.04	0.08	0.05	2.32	0.30	1.47	0.29
Brain	0.04	0.01	0.00	0.00	0.26	0.02	0.11	0.04
Tumor	7.54	0.97	2.62	0.65	11.23	1.18	6.50	1.19

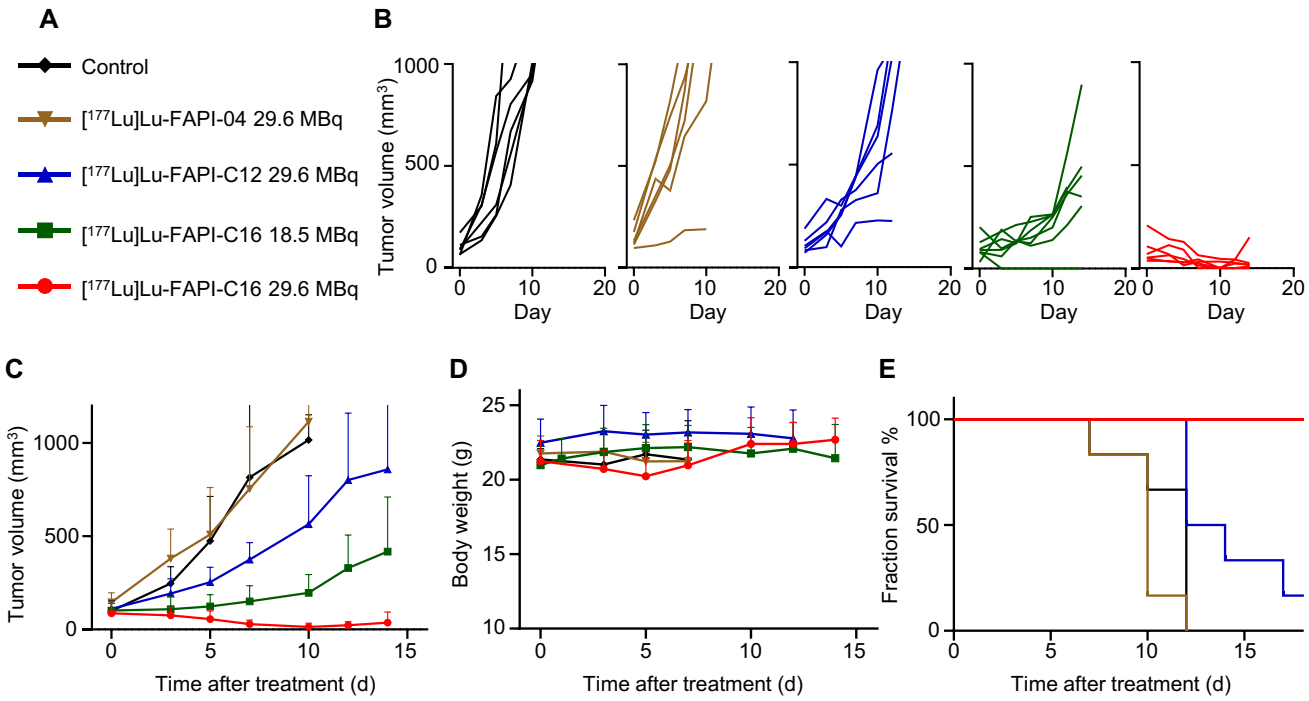

Fig. 8 Radionuclide therapy study of [^{177}Lu]Lu-FAPI-C12 and [^{177}Lu]Lu-FAPI-C16. **A** Design of therapy protocol ($n=6$); **B, C** tumor volume after treatment; **D** body weight change after treatment; **E** survival fraction after treatment

uptake than [^{177}Lu]Lu-FAPI-04 (Supplemental Figure 3 and Supplemental Table 1) at 24 h after injection, with the values of 11.22 ± 1.18%IA/g, 7.54 ± 0.97%IA/g, and 1.24 ± 0.54%IA/g, respectively, while for [^{177}Lu]Lu-FAPI-C16, it is worthy to note that higher liver, kidney, and lung uptakes were also observed at both 24 and 72 h.

Radionuclide therapy study

To evaluate and compare the antitumor efficacy of [^{177}Lu]Lu-FAPI-C12 and [^{177}Lu]Lu-FAPI-C16, a radionuclide therapy study was performed using HT-1080-FAP tumor-bearing mice. As illustrated in Fig. 8, the median survival of the [^{177}Lu]Lu-FAPI-04 treated group was only 10 days, and the radionuclide therapy efficacy had no significant difference with the saline-treated group of which the median survival was 12 days. For the group treated with 29.6 MBq [^{177}Lu]Lu-FAPI-C12, though there were better tumor growth inhibition results than that of the control and [^{177}Lu]Lu-FAPI-04 treated group, the median survival was 12 days which was similar to the other two groups. Significant tumor volume inhibition of [^{177}Lu]Lu-FAPI-C16 at the high activity of 29.6 MBq was observed, and the median survival was 28 days which was much longer than that of the [^{177}Lu]Lu-FAPI-04 treated group. When treated with the lower activity (18.5 MBq) of [^{177}Lu]Lu-FAPI-C16, the antitumor efficacy was impaired, and the median survival was 21 days which was still better than that of [^{177}Lu]Lu-FAPI-C12 using the high therapeutic activity of 29.6 MBq. Though transient weight loss was observed for the [^{177}Lu]Lu-FAPI-C16 high activity treatment group, the body weight recovered rapidly and then gained gradually. As shown in Supplemental Figure 7, histopathologic staining results of the main organs showed that there was also no obvious difference between the ^{177}Lu treated and control groups. Considering that the period was not long enough for histological side effect determination, further investigation will be performed in the following study for possible side effect monitoring.

Discussion

Conjugating fatty acid to FAPI may affect the binding affinity or selectivity to FAP. Therefore, the FAP specificity of FAPI-C12 and FAPI-C16 had been evaluated in vitro and in vivo. Binding affinity assays showed that the uptake of [^{68}Ga]Ga-FAPI-04 was notably reduced when incubated with 50 nM of unlabeled FAPI-C12 or FAPI-C16. The cell uptake of [^{68}Ga]Ga-FAPI-C12 and [^{68}Ga]Ga-FAPI-C16 in HT-1080-FAP cells was much higher than that in HT-1080-Vehicle cells which had no FAP expression. The above experiments indicated that the cell uptake of FAPI-C12 and FAPI-C16 depended on the FAP expression. According to the PET imaging in HT-1080-FAP and HT-1080-Vehicle

tumor-bearing mice, both [^{86}Y]Y-FAPI-C12 and [^{86}Y]Y-FAPI-C16 showed FAP expression-dependent uptake at 12 h, 24 h, and 48 h after injection, respectively. As FAPI clears overly rapidly, the blocking study was performed by pre-injection of FAPI-C16 and followed by sequential injection of [^{68}Ga]Ga-FAPI-04 at an indicated time point. The tumor uptake of [^{68}Ga]Ga-FAPI-04 could be inhibited as desired even at the later time point (i.e., 30 h). This result revealed that fatty acid-conjugated FAPI could bind FAP over a long period in the tumor; though it may be a dynamic process, it prolonged the tumor retention, and thus [^{177}Lu]Lu-FAPI-C16 provided notably better therapeutic efficacy than that of [^{177}Lu]Lu-FAPI-04. Though these two radiopharmaceuticals both had high FAP specificity in vitro and in vivo, their pharmacokinetic behaviors were different. Compared with radiolabeled FAPI-C16, radiolabeled FAPI-C12 cleared much faster, and the tumor retention also diminished accordingly. Though radiolabeled FAPI-C12 exhibited higher tumor uptake than that of radiolabeled FAPI-C16 within 1-h post-injection, the uptake quickly declined and became lower than that of radiolabeled FAPI-C16 after 1-h post-injection. This is of notable importance for tumor treatment. As shown in the head-to-head comparison radionuclide therapy study of these two radiopharmaceuticals, [^{177}Lu]Lu-FAPI-C16 showed significantly better therapeutic efficacy than that of [^{177}Lu]Lu-FAPI-C12 and [^{177}Lu]Lu-FAPI-04.

The long circulation is often a double-blade sword for developing radiopharmaceuticals. It may provide higher tumor accumulation, but may also raise the non-specific uptake in normal organs (e.g. liver), therefore giving unnecessary radiation does that may postpone the clinical translation. As the systemic circulation could be prolonged with the extension of the fatty acid chain, the variety of fatty acids provide us a window to optimize the chemical structure for radionuclide therapy efficiency improving while minimizing the radiation damage.

Conclusion

In this study, two fatty acid-conjugated FAPI radiopharmaceuticals are developed for the purpose to optimize the pharmacokinetics in vivo for radionuclide therapy. They both have excellent FAP specificity in vitro and in vivo, and compared with [^{177}Lu]Lu-FAPI-04, [^{177}Lu]Lu-FAPI-C12 and [^{177}Lu]Lu-FAPI-C16 achieve higher therapeutic dose delivery and enhanced radionuclide therapy efficiency. Considering that different alky chain length results the notable different metabolic properties, this study provides us guidance for further chemical structure optimization of FAPI-based radiopharmaceuticals to balance the radionuclide therapy efficiency and the possible side effect. In conclusion, the strategy of using fatty acids as an albumin binder may provide us a promising platform to transform rapid-clearing diagnostic radiotracers to long tumor retention therapeutic radiopharmaceuticals.

Supplementary Information The online version contains supplementary material available at https://doi.org/10.1007/s00259-021-05591-x.

Funding This work was funded by the Natural Science Foundation of Beijing, China (Grant No. Z200018), the National Science Foundation for Post-doctoral Scientists of China (Grant No. 2020M670047), the Special Foundation of Beijing Municipal Education Commission (Grant No. 3500–12020123), the National Natural Science Foundation of China (No. NSFC U1867209 and No. NSFC 21778003), and the Ministry of Science and Technology of the People's Republic of China (2017YFA0506300, 2020YFC2002702). Pu Zhang was supported in part by the Postdoctoral Fellowship of Peking-Tsinghua Center for Life Science.

Declarations

Ethics approval All animal care and experimental procedure were performed following the guidelines of the care and use of laboratory animals approved by the ethics committee of Peking University. This article does not contain any studies with human participants performed by any of the authors.

Conflict of interest Pu Zhang, Mengxin Xu, Junyi Chen, and Zhibo Liu are the consultant of Borui Biotech. Co. Ltd.

References

1. Xouri G, Christian S. Origin and function of tumor stroma fibroblasts. Semin Cell Dev Biol. 2010;21:40–6. https://doi.org/10.1016/j.semcdb.2009.11.017.
2. Eble JA, Niland S. The extracellular matrix in tumor progression and metastasis. Clin Exp Metastasis. 2019;36:171–98. https://doi.org/10.1007/s10585-019-09966-1.
3. Valkenburg KC, de Groot AE, Pienta KJ. Targeting the tumour stroma to improve cancer therapy. Nat Rev Clin Oncol. 2018;15:366–81. https://doi.org/10.1038/s41571-018-0007-1.
4. Östman A, Augsten M. Cancer-associated fibroblasts and tumor growth-bystanders turning into key players. Curr Opin Genet Dev. 2009;19:67–73. https://doi.org/10.1016/j.gde.2009.01.003.
5. Sahai E, Astsaturov I, Cukierman E, Denardo DG, Werb Z. A framework for advancing our understanding of cancer-associated fibroblasts. Nat Rev Cancer. 2020;20:1–13. https://doi.org/10.1038/s41568-019-0238-1.
6. Cirri P, Chiarugi P. Cancer associated fibroblasts: the dark side of the coin. Am J Cancer Res. 2011;1:482–97. https://doi.org/10.1016/B978-0-12-385524-4.00004-0.
7. Chen X, Song E. Turning foes to friends: targeting cancer-associated fibroblasts. Nat Rev Drug Discovery. 2019;18:99–115. https://doi.org/10.1038/s41573-018-0004-1.
8. Koustoulidou S, Hoorens M, Dalm SU, Mahajan S, Jong MD. Cancer-associated fibroblasts as players in cancer development and progression and their role in targeted radionuclide imaging and therapy. Cancers. 2021;13:1100. https://doi.org/10.3390/cancers13051100.

9. Park JE, Lenter MC, Zimmermann RN, Garin-Chesa P, Old LJ, Rettig WJ. Fibroblast activation protein, a dual specificity serine protease expressed in reactive human tumor stromal fibroblasts. J Cell Biochem. 1999;274:36505–12. https://doi.org/10.1074/jbc.274.51.36505.
10. Altmann A, Haberkorn U, Siveke J. The latest developments in imaging of fibroblast activation protein. J Nucl Med. 2021;62:160–7. https://doi.org/10.2967/jnumed.120.244806.
11. Busek P, Mateu R, Zubal M, Kotackova L, Sedo A. Targeting fibroblast activation protein in cancer-prospects and caveats. Front Biosci (Landmark Ed). 2018;23:1933–68.
12 Lindner T, Loktev A, Giesel F, Kratochwil C, Altmann A, Haberkorn U. Targeting of activated fibroblasts for imaging and therapy. EJNMMI Radiopharmacy Chem. 2019;4:1–15. https://doi.org/10.1186/s41181-019-0069-0.
13. Loktev A, Lindner T, Mier W, Debus J, Altmann A, Jäger D, et al. A tumor-imaging method targeting cancer-associated fibroblasts. J Nucl Med. 2018;59:1423–9. https://doi.org/10.2967/jnumed.118.210443.
14. Lindner T, Loktev A, Altmann A, Giesel F, Kratochwil C, Debus J, et al. Development of quinoline-based theranostic ligands for the targeting of fibroblast activation protein. J Nucl Med. 2018;59:1415–22. https://doi.org/10.2967/jnumed.118.210443.
15. Kratochwil C, Flechsig P, Lindner T, Abderrahim L, Altmann A, Mier W, et al. ^{68}Ga-FAPI PET/CT: tracer uptake in 28 different kinds of cancer. J Nucl Med. 2019;60:801–5. https://doi.org/10.2967/jnumed.119.227967.
16. Chen H, Pang Y, Wu J, Zhao L, Hao B, Wei J, et al. Comparison of [^{68}Ga]Ga-DOTA-FAPI-04 and [^{18}F]FDG PET/CT for the diagnosis of primary and metastatic lesions in patients with various types of cancer. Eur J Nucl Med Mol Imaging. 2020;47:1820–32. https://doi.org/10.1007/s00259-020-04769-z.
17. Giesel FL, Adeberg S, Syed M, Lindner T, Jiménez-Franco LD, Mavriopoulou E, et al. FAPI-74 PET/CT using either ^{18}F-AlF or cold-kit ^{68}Ga labeling: biodistribution, radiation dosimetry, and tumor delineation in lung cancer patients. J Nucl Med. 2021;62:201–7. https://doi.org/10.2967/jnumed.120.245084.
18. Loktev A, Lindner T, Burger EM, Altmann A, Giesel F, Kratochwil C, et al. Development of fibroblast activation protein-targeted radiotracers with improved tumor retention. J Nucl Med. 2019;60:1421–9. https://doi.org/10.2967/jnumed.118.224469.
19. Windisch P, Zwahlen DR, Koerber SA, Giesel FL, Debus J, Haberkorn U, et al. Clinical results of fibroblast activation protein (FAP) specific PET and implications for radiotherapy planning: systematic review. Cancers. 2020;12:2629. https://doi.org/10.3390/cancers12092629.
20. Zhang J, Hao W, Weiss OJ, Cheng Y, Niu G, Li F, et al. Safety, pharmacokinetics and dosimetry of a long-acting radiolabeled somatostatin analogue ^{177}Lu-DOTA-EB-TATE in patients with advanced metastatic neuroendocrine tumors. J Nucl Med. 2018;59:1699–705. https://doi.org/10.2967/jnumed.118.209841.
21. Jie Z, Fan X, Wang H, Liu Q, Wang J, Li H, et al. First-in-human study of ^{177}Lu-EB-PSMA-617 in patients with metastatic castration-resistant prostate cancer. Eur J Nucl Med Mol Imaging. 2019;46:148–58. https://doi.org/10.1007/s00259-018-4096-y.
22. Kramer V, Fernández R, Lehnert W, Jiménez-Franco LD, Soza-Ried C, Eppard E, et al. Biodistribution and dosimetry of a single dose of albumin-binding ligand [^{177}Lu]Lu-PSMA-ALB-56 in patients with mCRPC. Eur J Nucl Med Mol Imaging. 2021;48:893–903. https://doi.org/10.1007/s00259-020-05022-3.
23. Kuo HT, Lin KS, Zhang Z, Uribe CF, Merkens H, Zhang C, et al. ^{177}Lu-labeled albumin-binder-conjugated PSMA-targeting agents with extremely high tumor uptake and enhanced tumor-to-kidney absorbed dose ratio. J Nucl Med. 2021;62:521–7. https://doi.org/10.2967/jnumed.120.250738.
24. Liu Z, Chen X. Simple bioconjugate chemistry serves great clinical advances: albumin as a versatile platform for diagnosis and precision therapy. Chem Soc Rev. 2016;45:1432–56. https://doi.org/10.1039/c5cs00158g.
25. Drucker DJ, Dritselis A, Kirkpatrick P. Liraglutide. Nat Rev Drug Discovery. 2010;9:267–8. https://doi.org/10.1038/nrd3148.
26. Elbrønd B, Jakobsen G, Larsen S, Agerso H, Jensen LB, Rolan P, et al. Pharmacokinetics, pharmacodynamics, safety, and tolerability of a single-dose of NN2211, a long-acting glucagon-like peptide 1 derivative, in healthy male subjects. Diabetes Care. 2002;25:1398–404. https://doi.org/10.2337/diacare.25.8.1398.
27. Knudsen LB, Lau J. The discovery and development of liraglutide and semaglutide. Front Endocrinol. 2019;10:1–32. https://doi.org/10.3389/fendo.2019.00155.
28. Madsen K, Knudsen LB, Agersoe H, Nielsen PF, Thøgersen H, Wilken M, et al. Structure-activity and protraction relationship of long-acting glucagon-like peptide-1 derivatives: importance of fatty acid length, polarity, and bulkiness. J Med Chem. 2007;50:6126–32. https://doi.org/10.1021/jm070861j.
29. Kenyon MA, Hamilton JA. ^{13}C NMR studies of the binding of medium-chain fatty acids to human serum albumin. J Lipid Res. 1994;35:458–67. https://doi.org/10.1016/S0022-2275(20)41196-4.
30. Wang Q, Wang Y, Ding J, Wang C, Zhou X, Gao W, et al. A bioorthogonal system reveals antitumour immune function of pyroptosis. Nature. 2020;579:421–6. https://doi.org/10.1038/s41586-020-2079-1.
31. Avila-Rodriguez MA, Nye JA, Nickles RJ. Production and separation of non-carrier-added ^{86}Y from enriched ^{86}Sr targets. Appl Radiat Isot. 2008;66:9–13. https://doi.org/10.1016/j.apradiso.2007.07.027.
32. Ren J, Xu M, Chen J, Ding J, Wang P, Huo L, et al. PET imaging facilitates antibody screening for synergistic radioimmunotherapy with a ^{177}Lu-labeled αPD-L1 antibody. Theranostics. 2021;11:304–15. https://doi.org/10.7150/thno.45540.